HHS Public Access

Author manuscript

*Metabolism*. Author manuscript; available in PMC 2024 November 01.

Published in final edited form as:

*Metabolism*. 2023 November ; 148: 155693. doi:10.1016/j.metabol.2023.155693.

# ATG14 plays a critical role in hepatic lipid droplet homeostasis

**Menghao Huang**[1], **Yang Zhang**[1], **Jimin Park**[1], **Kushan Chowdhury**[1], **Jiazhi Xu**[1], **Alex Lu**[2], **Lu Wang**[1], **Wenjun Zhang**[3], **Burcin Ekser**[3], **Liqing Yu**[4], **X. Charlie Dong**[1,5,6]

[1]Department of Biochemistry and Molecular Biology, Indiana University School of Medicine, Indianapolis, IN, USA;

[2]Park Tudor School, Indianapolis, IN, USA;

[3]Department of Surgery, Indiana University School of Medicine, Indianapolis, IN, USA;

[4]Department of Medicine, University of Maryland School of Medicine, Baltimore, MD, USA;

[5]Center for Computational Biology and Bioinformatics, Indiana University School of Medicine, Indianapolis, IN, USA;

[6]Center for Diabetes and Metabolic Diseases, Indiana University School of Medicine, Indianapolis, IN, USA.

## Abstract

**Background & Aims:** Autophagy-related 14 (ATG14) is a key regulator of autophagy. ATG14 is also localized to lipid droplet; however, the function of ATG14 on lipid droplet remains unclear. In this study, we aimed to elucidate the role of ATG14 in lipid droplet homeostasis.

**Methods:** ATG14 loss-of-function and gain-of-function in lipid droplet metabolism were analyzed by fluorescence imaging in ATG14 knockdown or overexpression hepatocytes. Specific domains involved in the ATG14 targeting to lipid droplets were analyzed by deletion or site-specific mutagenesis. ATG14-interacting proteins were analyzed by co-immunoprecipitation. The

**Corresponding author:** X. Charlie Dong, PhD, 635 Barnhill Drive, MS 1021D, Indianapolis, IN 46202, USA, xcdong@iu.edu, Phone: 317-278-1097.

Author contributions

MH performed experiments, data analysis, and manuscript writing; YZ, JP, KC, JX, AL, and LW performed experiments; WZ and BE provided human samples and revised the manuscript; LY provided an animal model; XCD designed the project, analyzed and interpreted the data, and wrote the manuscript.



Declaration of competing interest

The authors declare no competing interest.

Appendix A. Supplementary data

Credit Author Statement

**Menghao Huang**: Investigation, Data curation, Formal analysis, Writing – original draft. **Yang Zhang**: Investigation, Data curation, Formal analysis. **Jimin Park**: Investigation, Data curation. **Kushan Chowdhury**: Investigation, Data curation. **Jiazhi Xu**: Investigation. **Alex Lu**: Investigation. **Lu Wang**: Investigation. **Wenjun Zhang**: Investigation. **Burcin Ekser**: Investigation, Writing – review & editing. **Liqing Yu**: Investigation, Writing – review & editing. **X. Charlie Dong**: Investigation, Data curation, Formal analysis, Writing – original draft, review and editing.

Declaration of interest statement

None

effect of ATG14 on lipolysis was analyzed in human hepatocytes and mouse livers that were deficient in ATG14, comparative gene identification-58 (CGI-58), or both.

**Results:** Our data show that ATG14 is enriched on lipid droplets in hepatocytes. Mutagenesis analysis reveals that the Barkor/ATG14 autophagosome targeting sequence (BATS) domain of ATG14 is responsible for the ATG14 localization to lipid droplets. Co-immunoprecipitation analysis illustrates that ATG14 interacts with adipose triglyceride lipase (ATGL) and CGI-58. Moreover, ATG14 also enhances the interaction between ATGL and CGI-58. *In vitro* lipolysis analysis demonstrates that ATG14 deficiency remarkably decreases triglyceride hydrolysis.

**Conclusions:** Our data suggest that ATG14 can directly enhance lipid droplet breakdown through interactions with ATGL and CGI-58.

## Graphical Abstract

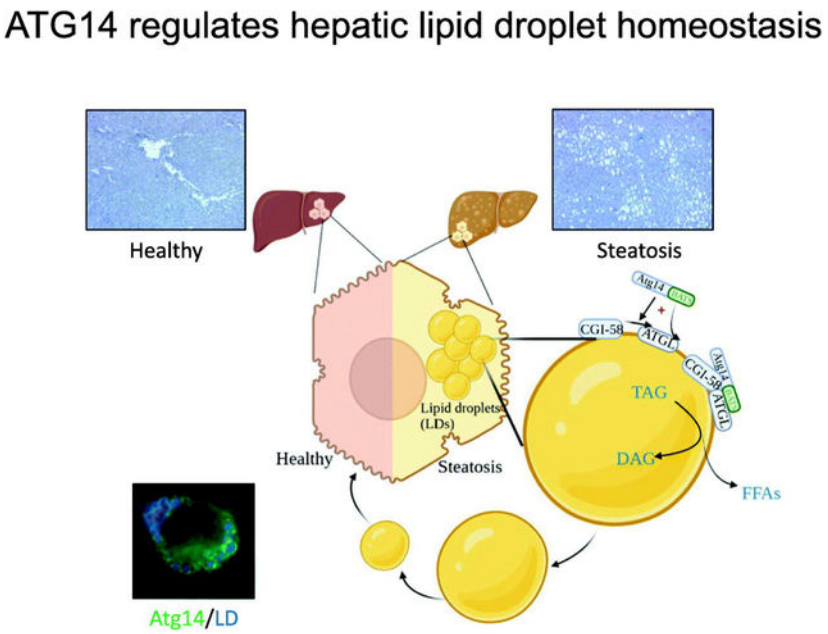


### Keywords

ATGL; ABHD5; CGI-58; lipolysis; autophagy

## 1. Introduction

Metabolic dysfunction-associated steatotic liver disease (MASLD) is a chronic liver disorder characterized by the presence of lipid droplets (LDs) in more than 5% of hepatocytes. Obesity, insulin resistance, and type 2 diabetes are major risk factors for MASLD [1–4]. Benign MASLD can progress to nonalcoholic steatohepatitis (NASH), characteristic of hepatic inflammation, ballooning, and fibrosis [1]. Accumulation of hepatic LDs often occurs because of dysregulated lipid metabolism. Under physiological conditions, LDs are metabolically active cellular organelles that store neutral lipids such as triglycerides (TG) and cholesterol esters and contribute critically to lipid and energy homeostasis. Two major metabolic pathways are involved in LD breakdown: neutral lipolysis and lipophagy. Adipose

triglyceride lipase (ATGL), encoded by the patatin-like phospholipase containing protein 2 (*PNPLA2*) gene, is the rate-limiting lipase in the TG hydrolysis in adipose tissue, muscle, and liver via the neutral lipolysis pathway [5–10]. Numerous proteins are known to interact and modulate the ATGL enzymatic activity. A key activator of ATGL is comparative gene identification 58 (CGI-58) encoded by the abhydrolase domain containing 5 (*ABHD5*) gene [11]. The dynamic interaction between ATGL and CGI-58 is regulated in part by perilipins including perilipin 1 (PLIN1) and PLIN5 [12]. Lipophagy is a specialized form of autophagy for the LD degradation [13–15]. Impaired hepatic autophagy has been implicated in the progression of MASLD [16–19].

Autophagy-related 14 (ATG14) is a key regulator of autophagy [20]. ATG14 interacts with Beclin 1 and vacuolar protein sorting 34 homolog (VPS34) to form the Class III phosphatidylinositol 3-kinase complex, which is involved in autophagosome formation [21, 22]. ATG14 protein has three coiled-coil domains (CCDs) in the amino terminal region, which are involved in protein-protein interactions [23]. The Barkor/ATG14 autophagosome targeting sequence (BATS) domain at the carboxyl terminal of ATG14 is known for membrane sensing and anchoring [23]. The evolutionarily conserved cysteines (C) at C43 and C46 in the amino region of ATG14 are involved in the ATG14 homo-oligomerization, which promotes membrane tethering and fusion of autophagosome to endolysosome [24]. Under starvation or nutrient-depletion conditions, ATG14 is localized at the endoplasmic reticulum (ER) for the early autophagosomal membrane formation [25]. Regardless of nutritional status, ATG14 also targets to LDs. However, the role of ATG14 on LD remains elusive. In this work, we attempted to illustrate the biochemical and physiological functions of ATG14 in LD homeostasis.

## 2. Methods

### 2.1 Animal models and diets

All animal experimental procedures were approved with the protocol number 21015 by the Institutional Animal Care and Use Committee (IACUC) of Indiana University School of Medicine following the guidelines for the care and use of laboratory animals by the National Institutes of Health (NIH). Mice were maintained in a 12:12 hour light:dark cycle in an animal facility at Indiana University School of Medicine. *Atg14* liver-specific knockout (LKO), *Cgi-58* LKO, and *Atg14/Cgi-58* double LKO mice were generated by crossing floxed mice with Alb-Cre mice (strain #003574 from the Jackson Laboratory). *Atg14* floxed mouse strain was generated in our laboratory, *Cgi-58/Abhd5* floxed mice were imported from Dr. Liqing Yu at the University of Maryland [26]. Mice were maintained on the C57BL6/J background. Animals were fed with either a control diet (Teklad Diets 2018SX: 24% calories from protein, 18% calories from fat, and 58% calories from carbohydrate) or high-fat diet (HFD, Research Diets D12492C, 20% calories from protein, 60% calories from fat, 20% calories from carbohydrates) for 4 weeks or 6 weeks [27]. Adeno-associated viral vectors (AAV8) carrying either control green fluorescent protein (GFP), Atg14, Atg14-shRNA, or GFP-shRNA driven by the human thyroxine-binding globulin (*TBG*) gene promoter were injected into mice at a dose of $2 \times 10^{11}$ genome copies per mouse via tail vein. At the end of the experiments, the animals were euthanized for blood and tissue

collection after 4 hours of fasting. Both males and females at age of 6–8 months were used for the experiments. Representative data from males were presented here.

### 2.2 Human liver specimens

Human liver samples were obtained from MASLD patients from the Department of Surgery of Indiana University School of Medicine. Paraffin-embedded liver sections from control and MASLD subjects were also obtained. The use of human samples was approved by the Institutional Review Board (IRB) at the Indiana University School of Medicine (IRB# 2007914455). The general characteristics of MASLD patients were described in Supplementary Table S1.

### 2.3 DNA constructs and mutagenesis

The coding sequences for mouse *Atg14*, human *CGI-58* and *ATGL*, and control *GFP* were cloned into a pcDNA3 vector (Invitrogen) with a Flag or hemagglutinin (HA) tag by PCR cloning. Mouse Atg14 C43A/C46A (cysteine to alanine mutations), coiled-coil domain deletion ($CCD^{\Delta}$), and BATS domain deletion ($BATS^{\Delta}$) mutations were generated using a Q5 Site-Directed Mutagenesis Kit (New England Biolabs). Single guide RNAs (sgRNAs) targeting human *ATG14*, *ATG5*, *ATG7*, *CGI-58*, and *ATGL* coding sequences were designed using the GPP sgRNA Designer on the Broad Institute website and cloned into a lentiCRISPRv2 vector as a gift from Dr. Feng Zhang (Addgene, Cambridge, MA; #52961; http://n2t.net/addgene:52961; RRID: Addgene_52961). The DNA oligonucleotide sequences were described in Supplementary Table S2. The cloning procedures were essentially same as described previously [28]. The recombinant DNA work was approved by the Indiana University Institutional Biosafety Committee.

### 2.4 Cell culture and free fatty acid (FFA) treatment

Huh-7 cells were cultured in Dulbecco's Modified Eagle medium (DMEM) supplemented with 10% fetal bovine serum (FBS) and penicillin/streptomycin (Thermo Fisher Scientific). ATG14, CGI-58, ATGL, and ATG14/CGI-58 deficient Huh-7 cells were generated by CRISPR/Cas9 as we described previously [29]. Cells were cultured in an incubator with 5% $CO_2$ at 37°C. To increase cellular LDs, cells were treated with 200 μM oleic acid (OA) or 350 μM palmitic acid (PA) and OA mix (1:2 ratio) for 48 hours. To prepare fatty acids solutions, fatty acid-free bovine serum albumin (BSA) was first dissolved in phosphate buffered saline (PBS) to make a final concentration of 20% BSA solution. Then, the BSA solution was filter-sterilized and used for conjugation to PA or OA. Stock PA and OA solutions were prepared in NaOH (1:1.2 molar ratio) to make a final concentration of 20 mM, followed by conjugation to BSA (3:1 molar ratio).

### 2.5 Microscopy analysis

Mouse liver tissue specimens were fixed by 10% formalin, followed by paraffin embedding and sectioning at the Indiana University Histology Core. Tissue sections (4-μm thick) were deparaffinized and then hydrated in xylenes and a graded series of ethanol concentrations, followed by hematoxylin and eosin (H&E) staining using a standard protocol. For immunohistochemistry (IHC) analysis, after deparaffination and hydration, liver sections

were heated in 1 mM EDTA buffer for antigen retrieval at 100 °C for 5 minutes, then treated with normal horse serum for 1 hour. Then the sections were incubated with specific antibodies at 4 °C overnight and further processed for staining as previously described [27]. For Oil Red O (ORO) staining, frozen liver tissue sections were air-dried for 30 minutes at room temperature and then fixed in ice-cold 10% formalin for 10 minutes. The fixed tissue sections were rinsed immediately in distilled water for 3 times and air-dried for 5 minutes. The tissue sections were incubated in 100% propylene glycol for 5 minutes and then stained in pre-warmed ORO solution for 7 minutes at 60 °C. The tissue sections were incubated in 85% propylene glycol solution for 5 minutes and rinsed with distilled water three times. The sections were counterstained with hematoxylin for 30 seconds before they were mounted with 50% glycerol solution for microscopy imaging. For immunofluorescence (IF) analysis, Huh-7 cells were grown in a glass-bottom dish and then fixed with 4% paraformaldehyde for 15 minutes at room temperature, followed by 3 times of PBS wash and then incubation with specific antibodies, 100 μM monodansylpentane (MDH), or 10 μM BODIPY (Thermo Fisher Scientific) as previously described [30]. Images for H&E or IHC staining were captured using a Leica microscope. IF images were obtained using a Zeiss fluorescence microscope with AxioVision Rel 4.8 software. Lipid droplet areas, IHC-positive, and IF-positive areas were quantified from five random fields per section using the ImageJ 1.53 software. The antibodies used in this work were described in Supplementary Table S3.

### 2.6 Protein analysis

Total protein extracts from tissues or cells were prepared using either tissue or cell lysis buffer, then the protein samples were further processed for immunoblotting as described previously [29]. Signals were detected by chemiluminescence with Pierce ECL Western Blotting substrate and scanned with a ChemiDoc MP System (Bio-Rad Laboratories). Images were analyzed using the ImageJ software for quantitative analysis. For immunoprecipitation (IP) or Co-IP experiments, equal amounts of protein lysates were incubated with 1 μg of specific antibodies. After 16 hours of incubation at 4 °C, protein A/G plus agarose was added and incubated at 4 °C for 3 hours. The antibodies used here were described in Supplementary Table S3.

### 2.7 mRNA analysis

Total RNAs were extracted from tissues or cells with TRI reagent (Sigma) and complementary DNA (cDNA) was synthesized from 1 μg of total RNA using a cDNA synthesis kit (Thermo Fisher Scientific) in a final volume of 20 μl. Real-time PCR was performed using SYBR green Master Mix (Thermo Fisher Scientific) in an Eppendorf Realplex PCR system. Gene expression was calculated using the $\Delta\Delta C_t$ method and normalized to an internal control gene of peptidylprolyl isomerase A (*Ppia*) as previously described [31]. PCR primer sequences were described in Supplementary Table S2.

### 2.8 Triglyceride and free fatty acid measurements

Hepatic lipids were extracted from liver or cell homogenates using the Folch method [32]. Hepatic and serum triglycerides (TG) and free fatty acids (FFA) were measured with commercial assay kits from Thermo Fisher Scientific and Wako USA, respectively.

### 2.9 *In vitro* triglyceride hydrolase activity analysis

Cell or tissue extracts were used for *in vitro* triglyceride hydrolase activity analysis as previously described [33]. Briefly, 0.32 mM trioleoylglycerol (TO), 10 μCi $^{3}$H-TO/ml, and 45 μM phosphatidylcholine/phosphatidylinositol were added to an organic solvent-resistant assay tube. After the solvents were completely dry, the substrate was dissolved in 0.1 M potassium phosphate buffer containing 5% fatty acid-free BSA. 100 μl tissue or cell extract was mixed with 100 μl of the substrate solution and incubated for 1 hour in a water bath at 37 °C under constant shaking. The reaction was terminated by adding 3.25 ml of extraction solution I [Methanol/chloroform/*n*-heptane with a ratio of 10:9:7 (v/v/v)], followed by adding 1.05 ml of extraction solution II (0.1 M potassium carbonate, pH 10.5) and mixing vigorously for 5 seconds on a vortex. After centrifugation at 1000 × g for 10 minutes, 200 μl of the upper aqueous phase was transferred to a scintillation vial containing 2 ml of scintillation cocktail and radioactivity was measured by a scintillation counter. Triglyceride hydrolase activity was calculated as nmol fatty acids per mg protein per hour of reaction. Samples were measured in triplicates.

### 2.10 Statistical analysis

All statistical data were expressed as mean ± SEM. Statistical analysis was performed using Prism 10 software (GraphPad). Comparisons between two groups were performed using a two-tailed unpaired Student *t*-test and comparisons for more than two groups were performed using a one-way analysis of variance followed by the Tukey post-hoc test.

## 3. Results

### 3.1 Hepatic ATG14 is decreased in MASLD/NASH

To examine whether autophagy is altered in the liver of MASLD patients, we performed immunoblot analysis of several autophagy-related proteins in human liver samples from early-stage steatosis and NASH patients. As expected, autophagy was impaired in the NASH livers compared to early-stage steatotic livers, evidenced by a decrease in microtubule-associated protein 1 light chain 3 (MAP1LC3, also commonly known as LC3) II:I ratio and a increase in sequestosome 1 (SQSTM1, also commonly known as p62). ATG5, ATG7, and ATG14 protein levels were decreased in the NASH livers compared to the steatotic livers. Lipolysis-related proteins CGI-58 and ATGL had no significant differences between the steatotic and NASH liver samples (Fig. 1A, B). In addition, H&E staining and hepatic TG measurements confirmed hepatic steatosis and IHC analysis revealed a significant decrease of ATG14 protein in the NASH livers (Fig. 1C, D).

To further verify the alteration of autophagy in an MASLD animal model, we challenged wild-type (WT) C57BL6/J mice with an HFD for 6 weeks. H&E staining and TG measurements confirmed hepatic steatosis in the HFD-treated mice (Fig. 2A–C). Real-time PCR analysis showed that hepatic mRNA levels of several autophagy-related genes including *Map1lc3b*, *Atg5*, *Atg7*, and *Atg14* were significantly decreased whereas there was no significant difference in *Cgi-58* and *Atgl* mRNA levels in the HFD-treated mouse livers compared to chow-fed mouse livers (Fig. 2D). Hepatic Atg14, Atg5, and Atg7 protein levels were significantly decreased in the HFD-treated mouse livers compared to chow-fed

livers. As expected, LC3 II:I ratio was decreased and p62 protein levels was increased in the HFD-treated mouse livers (Fig. 2E, F).

### 3.2 Atg14 protects against hepatic steatosis

To further investigate the effect of hepatic Atg14 deficiency on the development of MASLD, we knocked down hepatic Atg14 using AAV8-mediated shRNA in WT mice, then challenged them with an HFD for 4 weeks. Atg14 protein was significantly decreased in the Atg14 knockdown (KD) livers compared to control shGFP livers (Fig. 3A). Autophagy was impaired as indicated by elevated p62 protein levels and reduced LC3 II:I ratios (Fig. 3A). IHC analysis of p62 also confirmed impaired autophagy in the Atg14 KD livers (Fig. 3B). Atg14 KD mice had enlarged liver and increased liver to body weight ratios (Fig. S1A–C). Serum alanine aminotransferase (ALT), TG, and FFA levels were elevated in the Atg14 KD mice (Fig. S1D–F). Hepatic FFAs were also significantly increased in the Atg14 KD mice (Fig. S1G). Hepatic steatosis was much worse in the Atg14 KD mice than that in the control mice on the HFD diet as indicated by H&E staining, ORO staining, and TG measurements (Fig. 3C). Atg14 KD also led to moderate hepatic steatosis in chow-fed mice (Fig. 3D). To further verify the role of Atg14 in hepatic lipid homeostasis, we used AAV8 to overexpress Atg14 in the liver of WT mice. After 4 weeks of HFD feeding, we observed that Atg14 overexpression significantly reduced hepatic lipid droplets by H&E and ORO staining and TG measurements (Fig. 4A, B). Despite no change in body weight, liver weight and liver to body weight ratios were significantly decreased in the Atg14 overexpression mice (Fig. S2A–C). Serum ALT, TG, and FFA levels were decreased in the Atg14 overexpression mice (Fig. S2D–F). Hepatic FFA levels were also decreased in the Atg14 overexpression mice (Fig. S2G). Immunoblot analysis showed that overexpression of Atg14 in the liver enhanced autophagy as indicated by a remarkable decrease in p62 and an increase in LC3 II:I ratios. In contrast, Atg5, Atg7, Cgi-58, and Atgl protein levels were not significantly different between control and Atg14-overexpressed livers (Fig. 4C, D).

Next, we further confirmed the role of ATG14 in a human hepatocyte cell line Huh-7. Overexpression of ATG14 in Huh-7 cells significantly reduced p62 and increased LC3 II:I ratios whereas ATG14 knockdown by CRISPR/Cas9 markedly increased p62 and decreased LC3 II:I ratios (Fig. 4E). To assess autophagic flux, we also treated Huh-7 cells with an autophagy inhibitor — chloroquine. Consistently, ATG14 overexpression markedly increased and ATG14 KD decreased autophagy, respectively (Fig. S3A, B). As a result, ATG14 overexpression decreased whereas ATG14 KD increased cellular TG and FFA levels (Fig. 4F and Fig. S3C).

### 3.3 ATG14 promotes ATGL and CGI-58 interactions on lipid droplet

ATG14 has been reported to localize on lipid droplets in an osteosarcoma cell line U2OS [25]. However, the role of ATG14 in hepatic lipid droplet homeostasis is unclear. We first verified the subcellular localization of Atg14 in mouse liver by purification and analysis of hepatic lipid droplet proteins. Our data showed that Atg14 was present in both lipid droplet and cytosolic fractions as indicated by a lipid droplet marker Plin2 and a cytosolic marker β-actin (Fig. 5A). Moreover, IF analysis also showed that ATG14 was partially localized on lipid droplets indicated by a neutral lipid dye MDH in Huh-7 cells treated with 200 μM OA

(Fig. 5B). To examine whether ATG14 interacts with other lipid droplet-associated proteins, we co-transfected Flag-tagged ATGL, CGI-58, or ULK1 (Unc-51 like autophagy activating kinase 1) with HA-tagged ATG14 into Huh-7 cells. We pulled down protein complexes with HA antibodies and analyzed immunoprecipitated proteins by immunoblotting with Flag antibodies. Our data showed that ATG14 indeed interacted with ATGL and CGI-58 (ULK1 served as a positive control) (Fig. 5C). Additionally, Co-IP analysis using ATG14 antibody also showed that ATG14 interacted with ATGL and CGI-58 endogenously (Fig. S4A, ULK1 as a positive control). To further confirm the interactions between ATG14 with ATGL and CGI-58, we also performed IF staining of endogenous ATG14 with overexpressed Flag-ATGL or Flag-CGI-58 and endogenous ATGL or CGI-58 after Huh-7 cells were treated with 350 μM of OA and PA mix. Our data showed that ATG14 had co-localization with ATGL and CGI-58 on lipid droplets (Fig. 5D and Fig. S4B). To further examine whether ATG14 has any effect on ATGL-interacting proteins, we performed Co-IP analysis of ATG14 overexpressed or KD Huh-7 cells using ATGL antibodies. Our data showed that ATG14 overexpression increased the interaction of ATGL with CGI-58 but decreased the interaction with G0S2 (G0/G1 switch 2) whereas ATG14 KD had the opposite effect (Fig. 5E).

### 3.4 The BATS domain of ATG14 is responsible for the interaction with ATGL on lipid droplet

To examine which domain or motif of ATG14 is responsible for its lipid droplet localization and interactions with ATGL and CGI-58, we generated several ATG14 mutants including C43A/C46A double mutations in the CXXC motif, CCD deletion, and BATS deletion. As expected, overexpression of any of those ATG14 mutants failed to enhance autophagy compared to wild-type ATG14 in Huh-7 cells indicated by p62 and LC3 II:I ratios (Fig. 6A). Interestingly, only the BATS deletion mutant lost interaction with ATGL and weakened the interaction between ATGL and CGI-58 whereas other ATG14 mutants retained the capability of interaction with ATGL (Fig. 6B). IF analysis also confirmed that the CCD deletion and C43A/C46A mutant ATG14 proteins could target to LD and were largely colocalized with ATGL whereas the BATS deletion ATG14 proteins were diffused and barely detected on LD (Fig. 6C). Neutral lipid staining and TG analysis also revealed that the CCD deletion and C43A/C46A mutants retained the partial function of lipid reduction whereas the BATS mutant lost most of the lipid-lowering effect in Huh-7 cells (Fig. 7A–C). These results suggest that the BATS domain of ATG14 is critical for the interaction with ATGL and enhancement of the ATGL and CGI-58 interaction. To test whether ATGL mediates the effect of ATG14 on hepatic lipid droplet metabolism, we overexpressed wild-type and mutant ATG14 in control or ATGL KD Huh-7 cells. Lipid droplet staining and cellular TG measurements showed that wild-type but not mutant ATG14 could significantly reduce neutral lipids (Fig. S5A, B). This suggests that ATG14 confers both ATGL-dependent and -independent effects on hepatic lipid droplet breakdown.

### 3.5 ATGL is indispensable for the lipid droplet localization of ATG14

As our data showed that ATG14 interacts with ATGL, we further examined whether ATG14 targeting LD requires the presence of ATGL. Fluorescence microscopy analysis showed that ATGL KD remarkably reduced ATG14 localization to LD whereas CGI-58 KD did not have

an obvious effect on the LD targeting of ATG14 (Fig. 8A–D). In addition, ATGL deficiency also markedly decreased the interaction between ATG14 and CGI-58 (Fig. 8E), suggesting that ATGL is a primary interacting partner with ATG14 on LD.

### 3.6 ATG14 promotes ATGL triglyceride hydrolase activity

To examine whether ATG14 has any effect on triglyceride hydrolysis, we performed *in vitro* TG hydrolase activity analysis. Our data showed that overexpression of WT, CCD deletion, and C43A/C46A mutant ATG14 enhanced TG hydrolase activities whereas overexpression of the BATS deletion mutant ATG14 had no effect on TG hydrolysis in Huh-7 cell extracts (Fig. 9A). To further verify this, we performed TG hydrolase activity assays in Huh-7 cells deficient in either ATG14, CGI-58, or both. Our data showed that ATG14 KD had a similar effect on the TG hydrolase activity to CGI-58 KD whereas ATG14/CGI-58 double KD had a more dramatic effect on the TG hydrolase activity (Fig. 9A). To corroborate this, we also performed TG hydrolase activity assays in liver lysates from Atg14-LKO, Cgi-58-LKO, and Atg14/Cgi-58 LDKO mice. Our data showed that there was a decrease of 52%, 59%, and 88% of the TG hydrolase activities in the liver of Atg14-LKO, Cgi-58-LKO, and Atg14/Cgi-58 LDKO mice, respectively (Fig. 9A). As a result, TG levels were increased in the Atg14, Cgi-58, and Atg14/Cgi-58 deficient cells and liver tissues (Fig. 9B, C).

Next, we assessed the contribution of autophagy to the ATG14-mediated TG hydrolysis. To inhibit autophagy, we knocked down *ATG5* or *ATG7* in Huh-7 cells using the CRISPR/Cas9 approach. As expected, *ATG5* or *ATG7* KD significantly impaired autophagy, indicated by elevated p62 protein and reduced LC3 II:I ratios (Fig. 10A–C). ATG14 overexpression was not able to rescue the impaired autophagy induced by ATG5 or ATG7 deficiency (Fig. 10D and Fig. S6A, B). Nevertheless, ATG14 overexpression was able to effectively reduce neutral lipids even in the ATG5 or ATG7 deficient cells (Fig. 10E, F). Similarly, TG hydrolysis enhancement by the ATG14 overexpression was not impaired by either ATG5 or ATG7 deficiency in Huh-7 cells (Fig. 10G).

## 4. Discussion

ATG14 has been largely implicated in the regulation of phagophore formation and autophagosome-endolysosome fusion through an interaction with the Beclin 1-VPS34 complex and syntaxin 17 (STX17), respectively [21, 22, 24, 34, 35]. In our previous work, we have shown that adenovirus-mediated Atg14 knockdown or overexpression in mouse livers significantly increases or decreases both hepatic and serum TG levels, respectively [36]. However, whether the Atg14 effect is dependent on autophagy or not has not been examined previously. Later, Pfisterer et al. have reported that ATG14 and ATG2A are localized on lipid droplets and knockdown of ATG14 or ATG2A by small interfering RNAs in HeLa cervical cancer cell line increased lipid droplet numbers regardless of starvation [25], suggesting that ATG14 and ATG2A might have autophagy-independent functions in lipid droplet metabolism. In this study, we have indeed identified an unconventional function of ATG14 in lipid droplet breakdown through direct regulation of the ATGL enzymatic activity.

The role of ATGL in hepatic triglyceride metabolism has been well studied. Adenoviral overexpression of ATGL in mouse livers significantly reduces hepatic TG levels and LD sizes [9]. Adenoviral overexpression of ATGL in ob/ob mice for 8 days leads to a decrease in hepatic TG by 65% compared to the control group [37]. Albumin-Cre mediated *Atgl* liver-specific knockout mice manifest progressive periportal macrovesicular and pericentral microvesicular hepatic steatosis and a decrease of 65% hepatic TG hydrolase activity compared to WT mice [10]. Adenovirus-mediated *Atgl* knockdown in mouse livers also leads to hepatic steatosis with more than 2-fold increase in hepatic TG levels and a decrease of ~40% hepatic TG hydrolase activity compared to the control group after 7 days of viral transduction [8]. Multiple factors have been reported to modulate the ATGL enzymatic activity, including activators such as CGI-58 and inhibitors like perilipins and G0S2 [11, 38–44]. The findings from this work suggest that ATG14 enhances the interaction between ATGL and CGI-58 but inhibits G0S2 from interacting with ATGL. In doing so, ATGL hydrolase activity can be enhanced.

Since lipophagy mediated by macrophage was documented a decade ago [13], the understanding of LD metabolism has been deepened substantially. Now it is known that LD contents can be directly transferred to the lysosome for breakdown without involvement of the autophagosome [15]. More importantly, an increasing number of studies have revealed that neutral lipolysis and lipophagy are interconnected. In primary rat hepatocytes, inhibition of lipophagy (by chloroquine, an autophagy inhibitor), lipoplysis (by atglistatin, an ATGL inhibitor), or both results in comparable LD contents but different LD sizes. ATGL inhibition leads to larger cytoplasmic LDs whereas autophagy inhibition results in an accumulation of smaller LDs in the cytoplasm and degradative acidic vesicles [45]. Chaperone-mediated autophagy can target LD-coating PLIN2 and PLIN3 for degradation, and subsequently ATGL and autophagy-related proteins such as ATG5, LC3, and Beclin 1 are increased on lipid droplets to promote both lipolysis and lipophagy in rat livers [14]. Liver-specific *Plin2* knockout mice are resistant to diet-induced hepatic steatosis. In the *Plin2* knockout primary mouse hepatocytes, inhibition of autophagy with chloroquine or ATGL with atglistatin or both results in similar reduction of cellular fatty acid oxidation, suggesting that ATGL and autophagy act through a common mechanism on cellular fatty acid oxidation [46]. ATGL can interact with LC3 through an LC3-interacting region (LIR) motif. Mutation of a single LIR motif in ATGL abolishes its LD association, suggesting that LC3 is a recruiter of ATGL to LD for lipolysis [47]. Additionally, ATGL is also necessary and sufficient for the induction of lipophagy partly mediated by sirtuin 1 [48]. The data from this work also reveals another layer of coordination of lipolysis and lipophagy as ATG14 can enhance both pathways to maintain hepatic LD homeostasis (Fig. S7). As ATG14 localizes to LD regardless of nutritional status, it suggests that ATG14 might be involved in the activation of basal lipolysis. Further investigation is needed to address the relative contribution of the basal LD breakdown to the overall energy homeostasis.

## 5. Conclusions

The findings from this work suggest an autophagy-independent function of ATG14 in the regulation of lipid droplet metabolism in the liver. Through interactions with both ATGL and CGI-58, ATG14 can enhance the ATGL-mediated lipolysis. As an endogenous activator of

both lipophagy and lipolysis, ATG14 could become a useful target for MASLD therapeutic development. Further investigation is needed to test this translational potential.

## Supplementary Material

Refer to Web version on PubMed Central for supplementary material.

## Acknowledgements

The authors want to thank Dr. Hyeong-Geug Kim, Jingru Liang, and Rachel Schweiger for the technical assistance.

### Funding

This work was supported in part by the National Institute of Diabetes and Digestive and Kidney Diseases (R01DK121925 and R01DK120689), the National Institute on Alcohol Abuse and Alcoholism (R01AA028506), and the National Institute on Aging (R21AG072288).

## Data statement

The data that support the findings in this study are available in the manuscript and supplementary appendix of this article.

## Abbreviations:

| | |
|---|---|
| **ABHD5** | abhydrolase domain containing 5 |
| **ATG14** | autophagy related 14 |
| **ATGL** | adipose triglyceride lipase |
| **BATS** | Barkor/ATG14 autophagosome targeting sequence |
| **CGI-58** | comparative gene identification-58 |
| **G0S2** | G0/G1 switch 2 |
| **LD** | lipid droplet |
| **MAP1LC3** | microtubule-associated protein 1 light chain 3 |
| **MASLD** | metabolic dysfunction-associated steatotic liver disease |
| **NASH** | nonalcoholic steatohepatitis |
| **PNPLA2** | patatin-like phospholipase containing protein 2 |
| **PPIA** | peptidylprolyl isomerase A |
| **SQSTM1** | sequestosome 1 |
| **STX17** | syntaxin 17 |
| **VPS34** | vacuolar protein sorting 34 homolog |

## References


[1]. Dong XC, Chowdhury K, Huang M, Kim HG. Signal Transduction and Molecular Regulation in Fatty Liver Disease. Antioxid Redox Signal. 2021;35:689–717. [PubMed: 33906425]

[2]. Younossi Z, Anstee QM, Marietti M, Hardy T, Henry L, Eslam M, et al. Global burden of NAFLD and NASH: trends, predictions, risk factors and prevention. Nat Rev Gastroenterol Hepatol. 2018;15:11–20. [PubMed: 28930295]

[3]. Haas JT, Francque S, Staels B. Pathophysiology and Mechanisms of Nonalcoholic Fatty Liver Disease. Annu Rev Physiol. 2016;78:181–205. [PubMed: 26667070]

[4]. Mashek DG, Khan SA, Sathyanarayan A, Ploeger JM, Franklin MP. Hepatic lipid droplet biology: Getting to the root of fatty liver. Hepatology. 2015;62:964–7. [PubMed: 25854913]

[5]. Li T, Guo W, Zhou Z. Adipose Triglyceride Lipase in Hepatic Physiology and Pathophysiology. Biomolecules. 2021;12.

[6]. Haemmerle G, Lass A, Zimmermann R, Gorkiewicz G, Meyer C, Rozman J, et al. Defective lipolysis and altered energy metabolism in mice lacking adipose triglyceride lipase. Science. 2006;312:734–7. [PubMed: 16675698]

[7]. Zimmermann R, Strauss JG, Haemmerle G, Schoiswohl G, Birner-Gruenberger R, Riederer M, et al. Fat mobilization in adipose tissue is promoted by adipose triglyceride lipase. Science. 2004;306:1383–6. [PubMed: 15550674]

[8]. Ong KT, Mashek MT, Bu SY, Greenberg AS, Mashek DG. Adipose triglyceride lipase is a major hepatic lipase that regulates triacylglycerol turnover and fatty acid signaling and partitioning. Hepatology. 2011;53:116–26. [PubMed: 20967758]

[9]. Turpin SM, Hoy AJ, Brown RD, Rudaz CG, Honeyman J, Matzaris M, et al. Adipose triacylglycerol lipase is a major regulator of hepatic lipid metabolism but not insulin sensitivity in mice. Diabetologia. 2011;54:146–56. [PubMed: 20842343]

[10]. Wu JW, Wang SP, Alvarez F, Casavant S, Gauthier N, Abed L, et al. Deficiency of liver adipose triglyceride lipase in mice causes progressive hepatic steatosis. Hepatology. 2011;54:122–32. [PubMed: 21465509]

[11]. Lass A, Zimmermann R, Haemmerle G, Riederer M, Schoiswohl G, Schweiger M, et al. Adipose triglyceride lipase-mediated lipolysis of cellular fat stores is activated by CGI-58 and defective in Chanarin-Dorfman Syndrome. Cell Metab. 2006;3:309–19. [PubMed: 16679289]

[12]. Sztalryd C, Brasaemle DL. The perilipin family of lipid droplet proteins: Gatekeepers of intracellular lipolysis. Biochim Biophys Acta. 2017;1862:1221–32.

[13]. Singh R, Kaushik S, Wang Y, Xiang Y, Novak I, Komatsu M, et al. Autophagy regulates lipid metabolism. Nature. 2009;458:1131–5. [PubMed: 19339967]

[14]. Kaushik S, Cuervo AM. Degradation of lipid droplet-associated proteins by chaperone-mediated autophagy facilitates lipolysis. Nat Cell Biol. 2015;17:759–70. [PubMed: 25961502]

[15]. Schulze RJ, Krueger EW, Weller SG, Johnson KM, Casey CA, Schott MB, et al. Direct lysosome-based autophagy of lipid droplets in hepatocytes. Proc Natl Acad Sci U S A. 2020;117:32443–52. [PubMed: 33288726]

[16]. Baselli GA, Jamialahmadi O, Pelusi S, Ciociola E, Malvestiti F, Saracino M, et al. Rare ATG7 genetic variants predispose patients to severe fatty liver disease. J Hepatol. 2022;77:596–606. [PubMed: 35405176]

[17]. An L, Wirth U, Koch D, Schirren M, Drefs M, Koliogiannis D, et al. Metabolic Role of Autophagy in the Pathogenesis and Development of NAFLD. Metabolites. 2023;13.

[18]. Lin CW, Zhang H, Li M, Xiong X, Chen X, Chen X, et al. Pharmacological promotion of autophagy alleviates steatosis and injury in alcoholic and non-alcoholic fatty liver conditions in mice. J Hepatol. 2013;58:993–9. [PubMed: 23339953]

[19]. Yang L, Li P, Fu S, Calay ES, Hotamisligil GS. Defective hepatic autophagy in obesity promotes ER stress and causes insulin resistance. Cell Metab. 2010;11:467–78. [PubMed: 20519119]

[20]. Sun Q, Fan W, Chen K, Ding X, Chen S, Zhong Q. Identification of Barkor as a mammalian autophagy-specific factor for Beclin 1 and class III phosphatidylinositol 3-kinase. Proc Natl Acad Sci U S A. 2008;105:19211–6. [PubMed: 19050071]

[21]. Zhong Y, Wang QJ, Li X, Yan Y, Backer JM, Chait BT, et al. Distinct regulation of autophagic activity by Atg14L and Rubicon associated with Beclin 1-phosphatidylinositol-3-kinase complex. Nat Cell Biol. 2009;11:468–76. [PubMed: 19270693]

[22]. Itakura E, Kishi C, Inoue K, Mizushima N. Beclin 1 forms two distinct phosphatidylinositol 3-kinase complexes with mammalian Atg14 and UVRAG. Mol Biol Cell. 2008;19:5360–72. [PubMed: 18843052]

[23]. Ohashi Y Activation Mechanisms of the VPS34 Complexes. Cells. 2021;10.

[24]. Diao J, Liu R, Rong Y, Zhao M, Zhang J, Lai Y, et al. ATG14 promotes membrane tethering and fusion of autophagosomes to endolysosomes. Nature. 2015;520:563–6. [PubMed: 25686604]

[25]. Pfisterer SG, Bakula D, Frickey T, Cezanne A, Brigger D, Tschan MP, et al. Lipid droplet and early autophagosomal membrane targeting of Atg2A and Atg14L in human tumor cells. J Lipid Res. 2014;55:1267–78. [PubMed: 24776541]

[26]. Guo F, Ma Y, Kadegowda AK, Betters JL, Xie P, Liu G, et al. Deficiency of liver Comparative Gene Identification-58 causes steatohepatitis and fibrosis in mice. J Lipid Res. 2013;54:2109–20. [PubMed: 23733885]

[27]. Huang M, Kim HG, Zhong X, Dong C, Zhang B, Fang Z, et al. Sestrin 3 Protects Against Diet-Induced Nonalcoholic Steatohepatitis in Mice Through Suppression of Transforming Growth Factor beta Signal Transduction. Hepatology. 2020;71:76–92. [PubMed: 31215672]

[28]. Zhong X, Huang M, Kim HG, Zhang Y, Chowdhury K, Cai W, et al. SIRT6 Protects Against Liver Fibrosis by Deacetylation and Suppression of SMAD3 in Hepatic Stellate Cells. Cell Mol Gastroenterol Hepatol. 2020;10:341–64. [PubMed: 32305562]

[29]. Chowdhury K, Huang M, Kim HG, Dong XC. Sirtuin 6 protects against hepatic fibrogenesis by suppressing the YAP and TAZ function. FASEB J. 2022;36:e22529. [PubMed: 36036554]

[30]. Zhu C, Huang M, Kim HG, Chowdhury K, Gao J, Liu S, et al. SIRT6 controls hepatic lipogenesis by suppressing LXR, ChREBP, and SREBP1. Biochim Biophys Acta Mol Basis Dis. 2021;1867:166249. [PubMed: 34425214]

[31]. Kim HG, Huang M, Xin Y, Zhang Y, Zhang X, Wang G, et al. The epigenetic regulator SIRT6 protects the liver from alcohol-induced tissue injury by reducing oxidative stress in mice. J Hepatol. 2019.

[32]. Folch J, Lees M, Sloane Stanley GH. A simple method for the isolation and purification of total lipides from animal tissues. J Biol Chem. 1957;226:497–509. [PubMed: 13428781]

[33]. Schweiger M, Eichmann TO, Taschler U, Zimmermann R, Zechner R, Lass A. Measurement of lipolysis. Methods Enzymol. 2014;538:171–93. [PubMed: 24529439]

[34]. Matsunaga K, Morita E, Saitoh T, Akira S, Ktistakis NT, Izumi T, et al. Autophagy requires endoplasmic reticulum targeting of the PI3-kinase complex via Atg14L. J Cell Biol. 2010;190:511–21. [PubMed: 20713597]

[35]. Fan W, Nassiri A, Zhong Q. Autophagosome targeting and membrane curvature sensing by Barkor/Atg14(L). Proc Natl Acad Sci U S A. 2011;108:7769–74. [PubMed: 21518905]

[36]. Xiong X, Tao R, DePinho RA, Dong XC. The autophagy-related gene 14 (Atg14) is regulated by forkhead box O transcription factors and circadian rhythms and plays a critical role in hepatic autophagy and lipid metabolism. J Biol Chem. 2012;287:39107–14. [PubMed: 22992773]

[37]. Reid BN, Ables GP, Otlivanchik OA, Schoiswohl G, Zechner R, Blaner WS, et al. Hepatic overexpression of hormone-sensitive lipase and adipose triglyceride lipase promotes fatty acid oxidation, stimulates direct release of free fatty acids, and ameliorates steatosis. J Biol Chem. 2008;283:13087–99. [PubMed: 18337240]

[38]. Lu X, Yang X, Liu J. Differential control of ATGL-mediated lipid droplet degradation by CGI-58 and G0S2. Cell Cycle. 2010;9:2719–25. [PubMed: 20676045]

[39]. Yang X, Lu X, Lombes M, Rha GB, Chi YI, Guerin TM, et al. The G(0)/G(1) switch gene 2 regulates adipose lipolysis through association with adipose triglyceride lipase. Cell Metab. 2010;11:194–205. [PubMed: 20197052]

[40]. Miyoshi H, Perfield JW 2nd, Souza SC, Shen WJ, Zhang HH, Stancheva ZS, et al. Control of adipose triglyceride lipase action by serine 517 of perilipin A globally regulates protein kinase A-stimulated lipolysis in adipocytes. J Biol Chem. 2007;282:996–1002. [PubMed: 17114792]

[41]. Bell M, Wang H, Chen H, McLenithan JC, Gong DW, Yang RZ, et al. Consequences of lipid droplet coat protein downregulation in liver cells: abnormal lipid droplet metabolism and induction of insulin resistance. Diabetes. 2008;57:2037–45. [PubMed: 18487449]

[42]. Granneman JG, Moore HP, Krishnamoorthy R, Rathod M. Perilipin controls lipolysis by regulating the interactions of AB-hydrolase containing 5 (Abhd5) and adipose triglyceride lipase (Atgl). J Biol Chem. 2009;284:34538–44. [PubMed: 19850935]

[43]. Granneman JG, Moore HP, Mottillo EP, Zhu Z, Zhou L. Interactions of perilipin-5 (Plin5) with adipose triglyceride lipase. J Biol Chem. 2011;286:5126–35. [PubMed: 21148142]

[44]. Wang H, Bell M, Sreenivasan U, Sreenevasan U, Hu H, Liu J, et al. Unique regulation of adipose triglyceride lipase (ATGL) by perilipin 5, a lipid droplet-associated protein. J Biol Chem. 2011;286:15707–15. [PubMed: 21393244]

[45]. Schott MB, Weller SG, Schulze RJ, Krueger EW, Drizyte-Miller K, Casey CA, et al. Lipid droplet size directs lipolysis and lipophagy catabolism in hepatocytes. J Cell Biol. 2019;218:3320–35. [PubMed: 31391210]

[46]. Griffin JD, Bejarano E, Wang XD, Greenberg AS. Integrated Action of Autophagy and Adipose Tissue Triglyceride Lipase Ameliorates Diet-Induced Hepatic Steatosis in Liver-Specific PLIN2 Knockout Mice. Cells. 2021;10.

[47]. Martinez-Lopez N, Garcia-Macia M, Sahu S, Athonvarangkul D, Liebling E, Merlo P, et al. Autophagy in the CNS and Periphery Coordinate Lipophagy and Lipolysis in the Brown Adipose Tissue and Liver. Cell Metab. 2016;23:113–27. [PubMed: 26698918]

[48]. Sathyanarayan A, Mashek MT, Mashek DG. ATGL Promotes Autophagy/Lipophagy via SIRT1 to Control Hepatic Lipid Droplet Catabolism. Cell reports. 2017;19:1–9. [PubMed: 28380348]

## Highlights

- ATG14 targets to lipid droplets in hepatocytes
- ATG14 interacts with ATGL and CGI-58
- ATG14 enhances the interaction between ATGL and CGI-58
- ATG14 has an autophagy-independent function in lipolysis

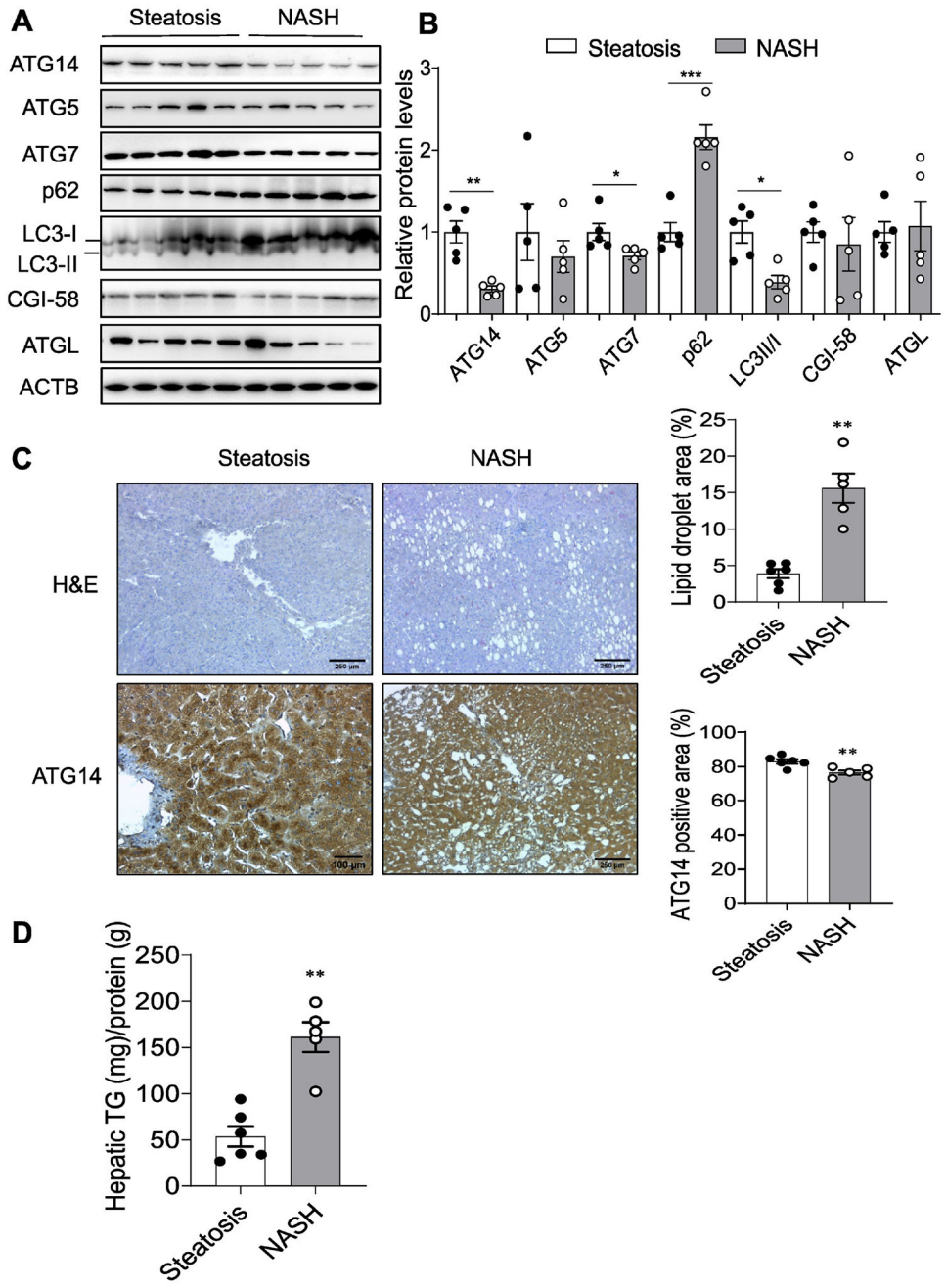


**Figure 1. Hepatic ATG14 is decreased in NASH patients.**

(A, B) Immunoblot and quantification analysis of ATG14, ATG5, ATG7, p62, LC3-I/II, CGI-58, and ATGL in liver samples from steatosis (n=5) and NASH patients (n=5). (C) H&E staining and ATG14 IHC analysis of the liver sections of steatosis and NASH patients. (D) Hepatic TG measurements from steatosis (n=6) and NASH patients (n=5). Data are presented as mean ± SEM. *P < 0.05, **P < 0.01, and ***P<0.001.

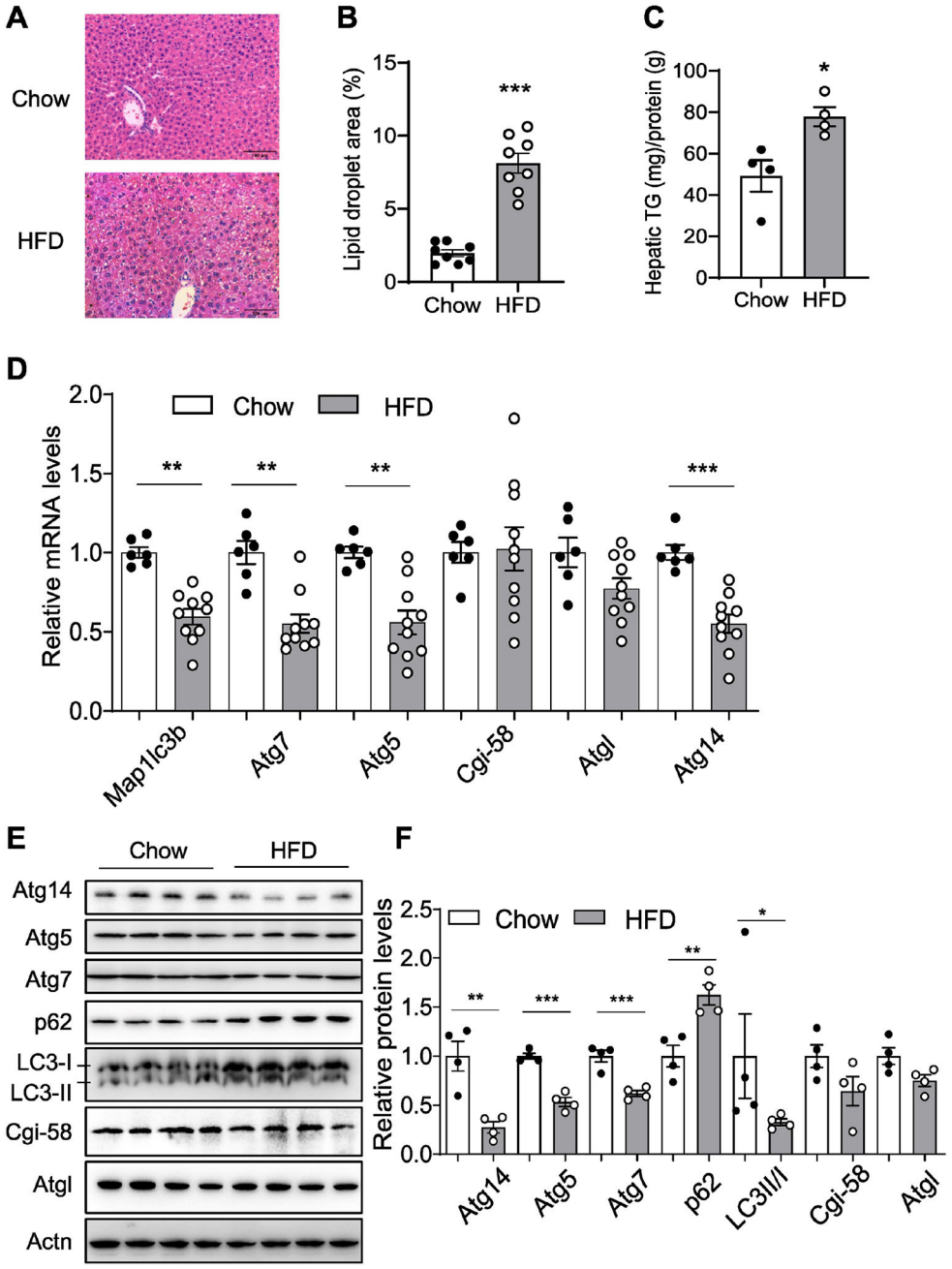


**Figure 2. Hepatic Atg14 is downregulated in diet-induced MASLD mice.**

(A, B) H&E staining and lipid droplet area quantification analysis of liver sections of WT male mice fed with chow or an HFD diet for 6 weeks (n=8). (C) Hepatic TG measurements from the chow and HFD diet-treated mice (n=4). (D) Real-time PCR analysis of expression of several autophagy-related genes including *Map1lc3b, Atg7, Atg5*, and *Atg14*, and lipolysis genes including *Cgi-58* and *Atgl* in the livers of WT mice fed with chow or an HFD diet for 6 weeks. (E, F) Immunoblot and quantification analysis of Atg14, Atg5, Atg7, p62, LC3-I/II, Cgi-58, and Atgl in livers of chow and HFD diet-treated mice (n=4). Data are presented as mean ± SEM. *P < 0.05, **P < 0.01, and ***P < 0.001.

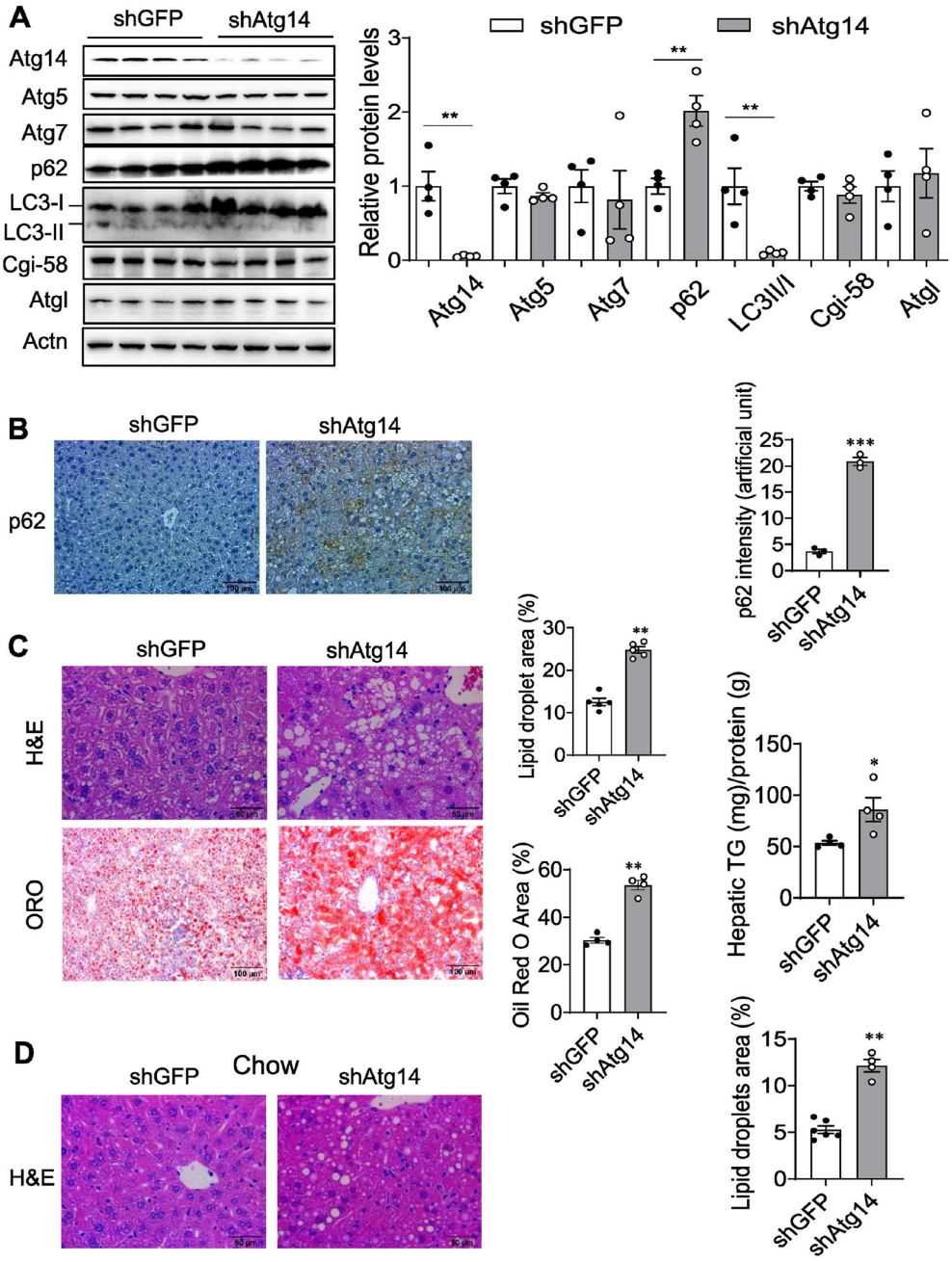


**Figure 3. Hepatic Atg14 deficient mice are more susceptible to diet-induced steatosis.**

(A) Immunoblot and quantification analysis of hepatic Atg14, Atg5, Atg7, p62, LC3-I/II, Cgi-58, and Atgl in either control GFP or Atg14 shRNA AAV8 injected male mice fed with an HFD for 4 weeks (n=4). (B) IHC and quantification analysis of p62 in liver sections of control and Atg14 knockdown mice (n=4). (C) H&E staining, Oil Red O staining, and TG measurements in control and Atg14 knockdown livers (n=4). (D) H&E staining and lipid droplet area quantification of liver sections of Atg14 shRNA or control shGFP AAV8 injected mice (n=4–6) fed with chow. Data are presented as mean ± SEM. *P < 0.05, **P < 0.01, and ***P < 0.001.

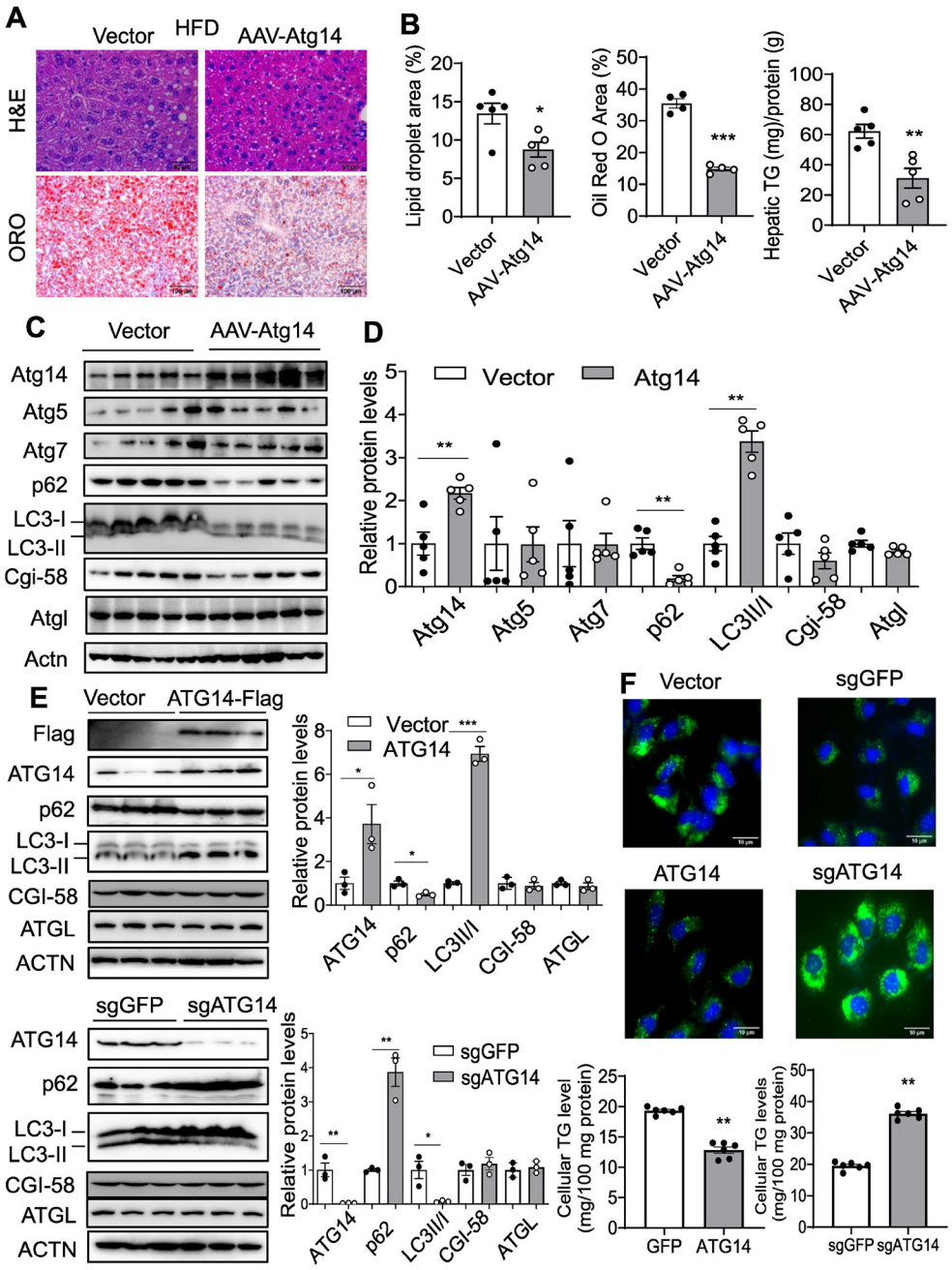


**Figure 4. Atg14 regulates hepatic autophagy and lipid droplets.**

(A, B) H&E and Oil Red O staining and hepatic TG measurements of livers of AAV8-Atg14 or AAV8-vector injected male mice (n=5) fed with an HFD diet for 4 weeks. (C, D) Immunoblot and quantification analysis of Atg14, Atg5, Atg7, p62, LC3-I/II, Cgi-58, and Atgl in AAV8-Atg14 or AAV8-vector injected mice that were treated with an HFD for 4 weeks (n=5). (E, F) Immunoblot and microscopy analysis of the effect of ATG14 overexpression or knockdown on autophagy and lipid droplets in Huh-7 cells transfected with corresponding plasmids. Lipid droplets were stained by BODIPY. Data are presented as mean ± SEM. *P < 0.05, **P < 0.01, and ***P < 0.001.

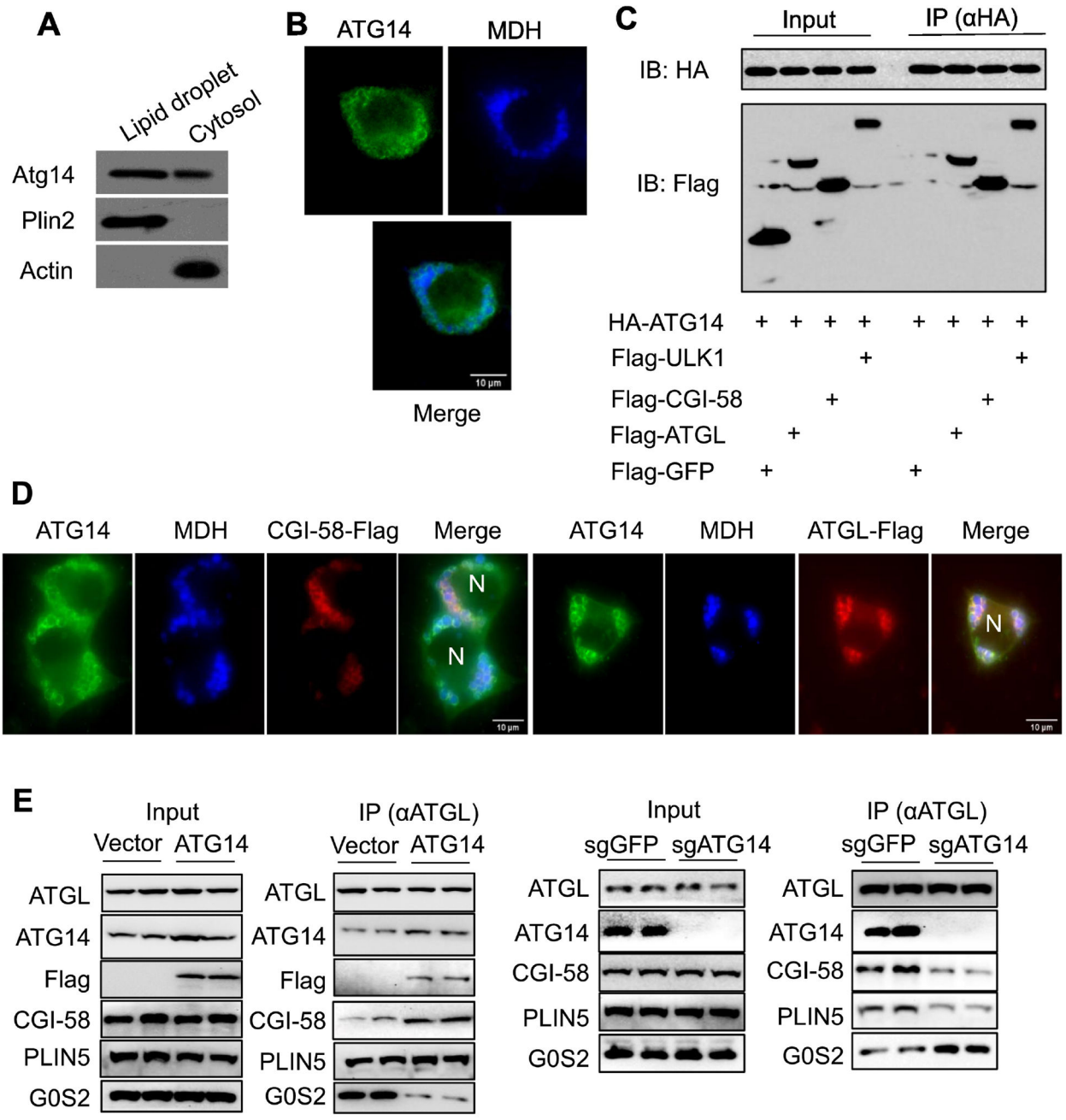


**Figure 5. ATG14 interacts with lipid droplet-associated proteins.**

(A) Immunoblot analysis of Atg14 in lipid droplet and cytosolic fractions of WT mouse liver tissue extract. (B) Immunofluorescence microscopy of endogenous ATG14 and lipid droplets in Huh-7 cells. (C) Co-IP analysis of potential interactions between ATG14 and ULK1 (a positive control), ATGL, or CGI-58 in Huh-7 cells. (D) Immunofluorescence microscopy of subcellular localization of ATG14, CGI-58-Flag, or ATGL-Flag in Huh-7 cells. (E) Co-IP analysis of ATGL-interacting proteins in Huh-7 cells that were transfected with vector, ATG14, sgGFP, or sgATG14 plasmids.

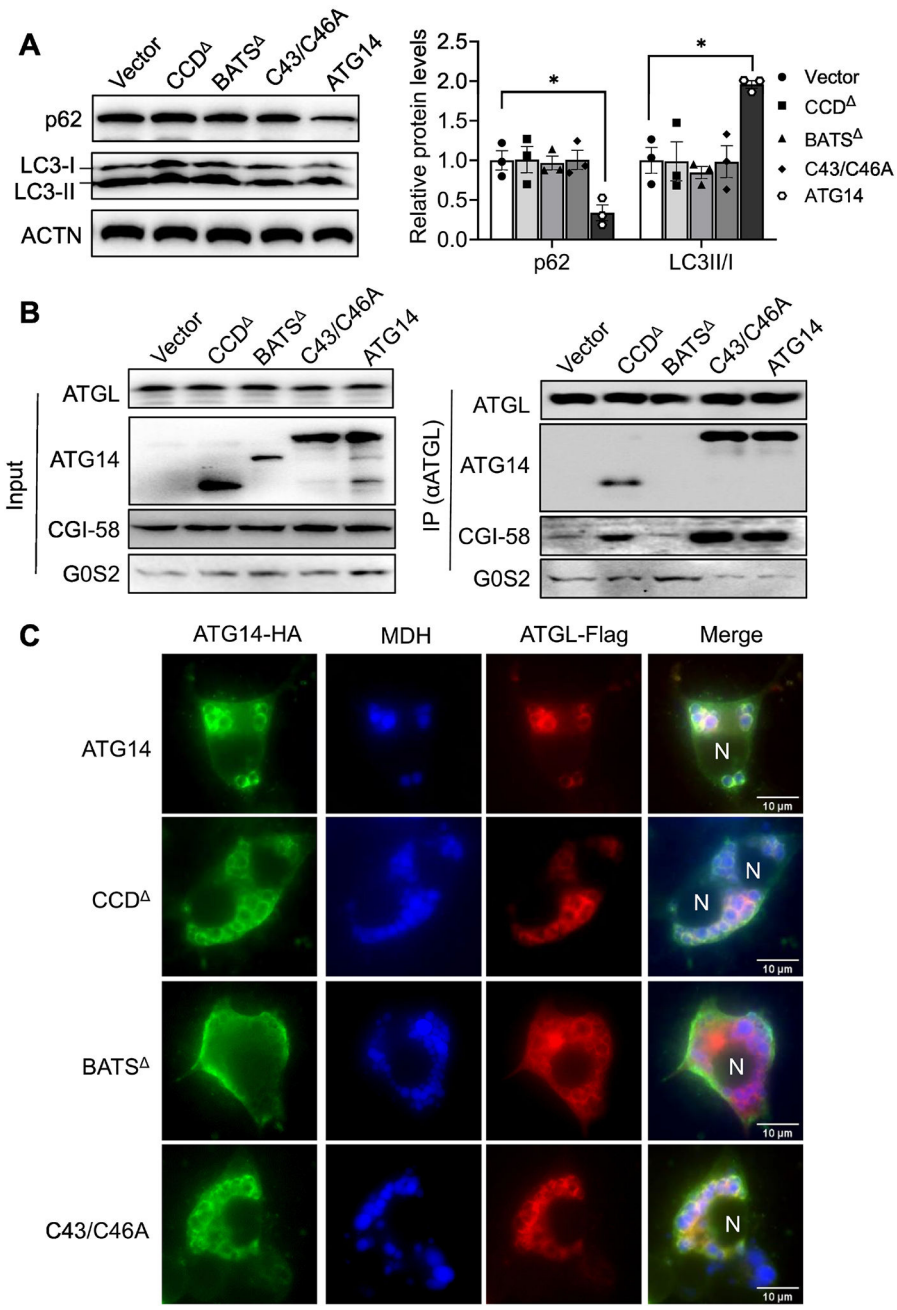


**Figure 6. The BATS domain of ATG14 is required for its interaction with ATGL on lipid droplets.**

(A) Immunoblot and quantification analysis of p62 and LC3-I/II in Huh-7 cells transfected with vector control, wild-type ATG14, CCD$^{\Delta}$, BATS$^{\Delta}$, or C43A/C46A mutant. (B) Co-IP analysis of interactions between ATGL and different ATG14 constructs in Huh-7 cells treated with 350 μM oleic acid and palmitic acid mix. (C) Immunofluorescence microscopy of subcellular localization of ATGL and different ATG14 constructs in Huh-7 cells treated with 350 μM oleic acid and palmitic acid mix. Data are presented as mean ± SEM. *P < 0.05.

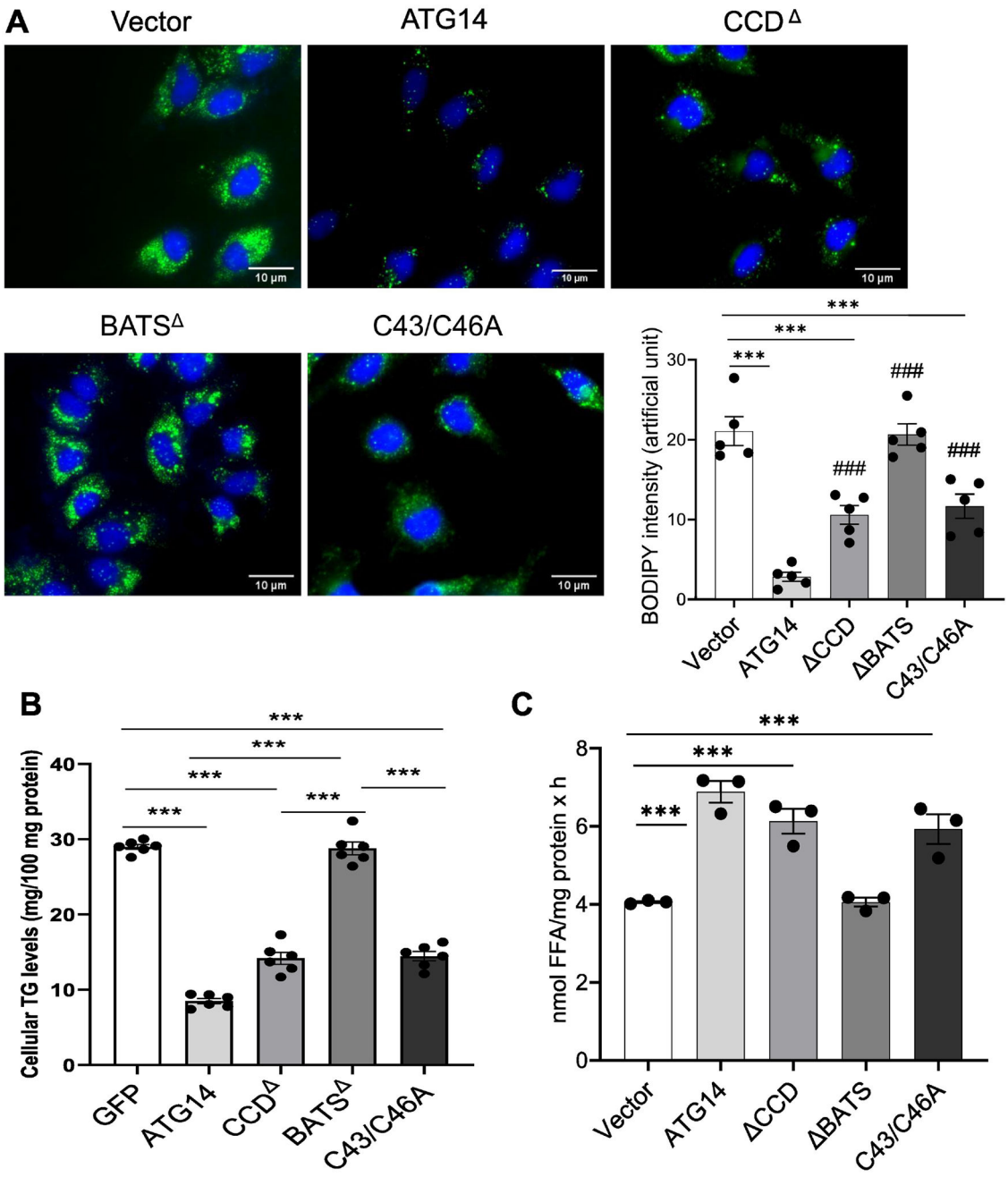


**Figure 7. ATG14 promotes lipolysis.**

(A-C) BODIPY staining, cellular TG measurements, and TG hydrolase activity analysis in Huh-7 cells transfected with wild-type or mutant ATG14 constructs. Data are presented as mean ± SEM. ***P < 0.001; ###P<0.001 vs. wild-type ATG14.

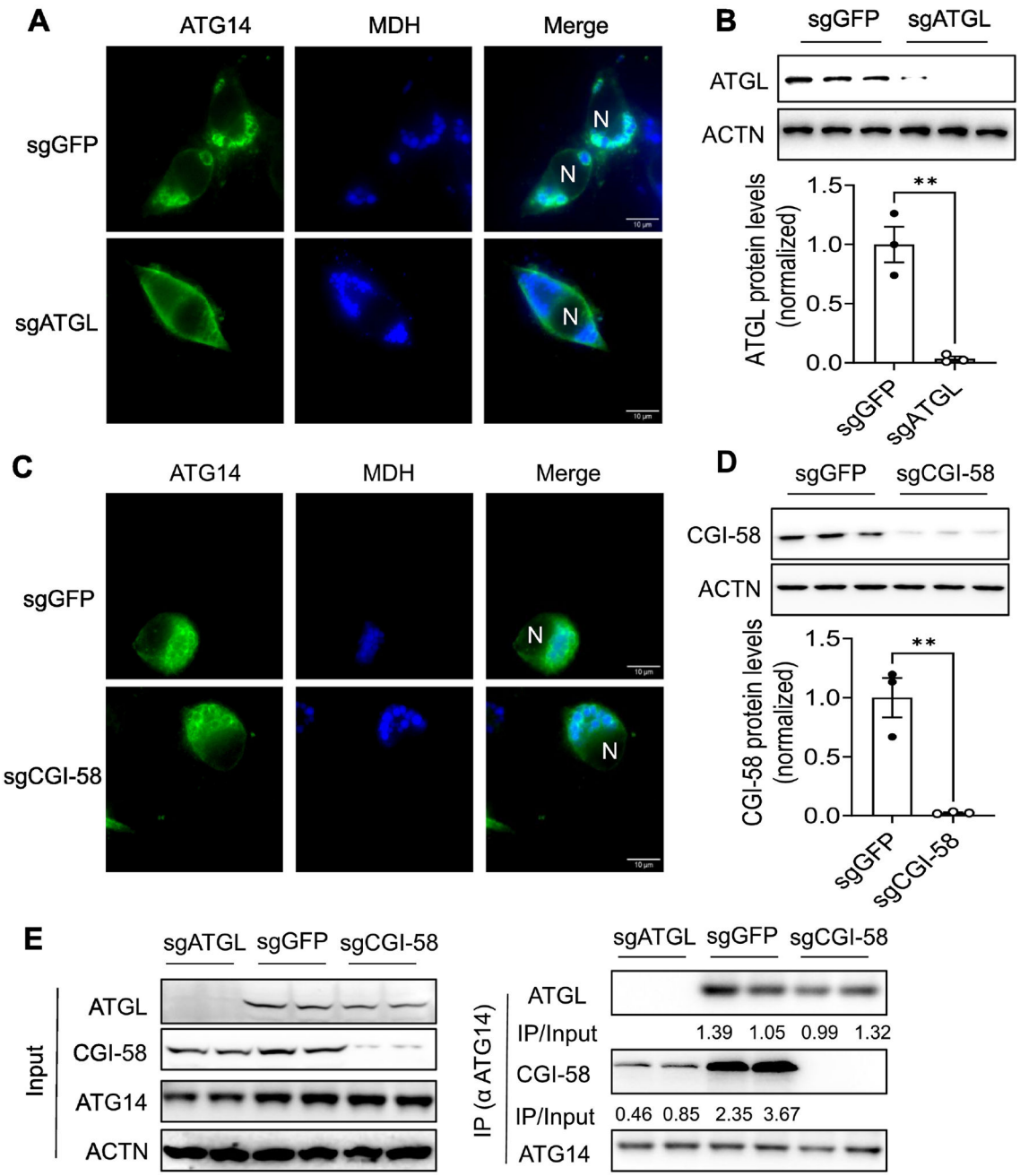


**Figure 8. ATGL is critical for the lipid droplet localization of ATG14 and its interaction with CGI-58.**

(A) Immunofluorescence microscopy of ATG14 subcellular localization in ATGL deficient Huh-7 cells treated with 350 μM oleic acid and palmitic acid mix. (B) Immunoblot and quantification analysis of ATGL in Huh-7 cells transfected with sgGFP and sgATGL. (C) Immunofluorescence microscopy of ATG14 subcellular localization in CGI-58 deficient Huh-7 cells treated with 350 μM oleic acid and palmitic acid mix. (D) Immunoblot and quantification analysis of CGI-58 in Huh-7 cells transfected with sgGFP and sgCGI-58. (E) Co-IP analysis of ATG14 interaction with ATGL or CGI-58 in ATGL or CGI-58 deficient

Huh-7 cells treated with 350 μM oleic acid and palmitic acid mix. Data are presented as mean ± SEM. **P < 0.01.

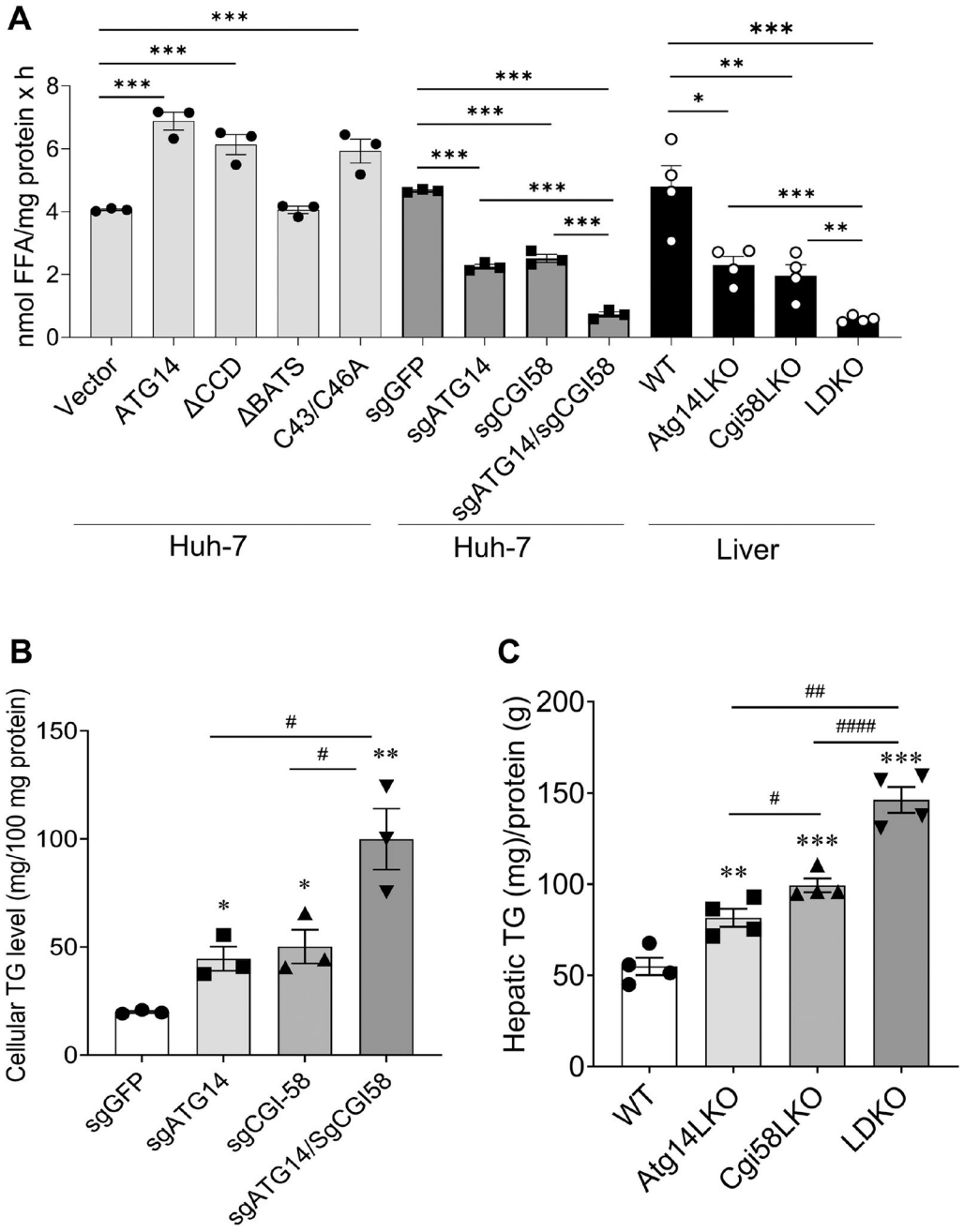


**Figure 9. ATG14 and CGI-58 have additive effects on lipolysis.**

(A) TG hydrolase activity was analyzed in Huh-7 cells transfected with different ATG14 constructs or CRISPR/Cas9 knockdown plasmids and mouse livers deficient in Atg14, Cgi-58, or both. (B, C) Cellular and hepatic TG levels were measured in Huh-7 cells or mouse livers deficient in Atg14, Cgi-58, or both (n=3–4). Data are presented as mean ± SEM. *P < 0.05, **P < 0.01 and ***P < 0.001 vs vector, sgGFP, or WT; $^{\#}$P < 0.05, $^{\#\#}$P < 0.01, and $^{\#\#\#}$P < 0.001.

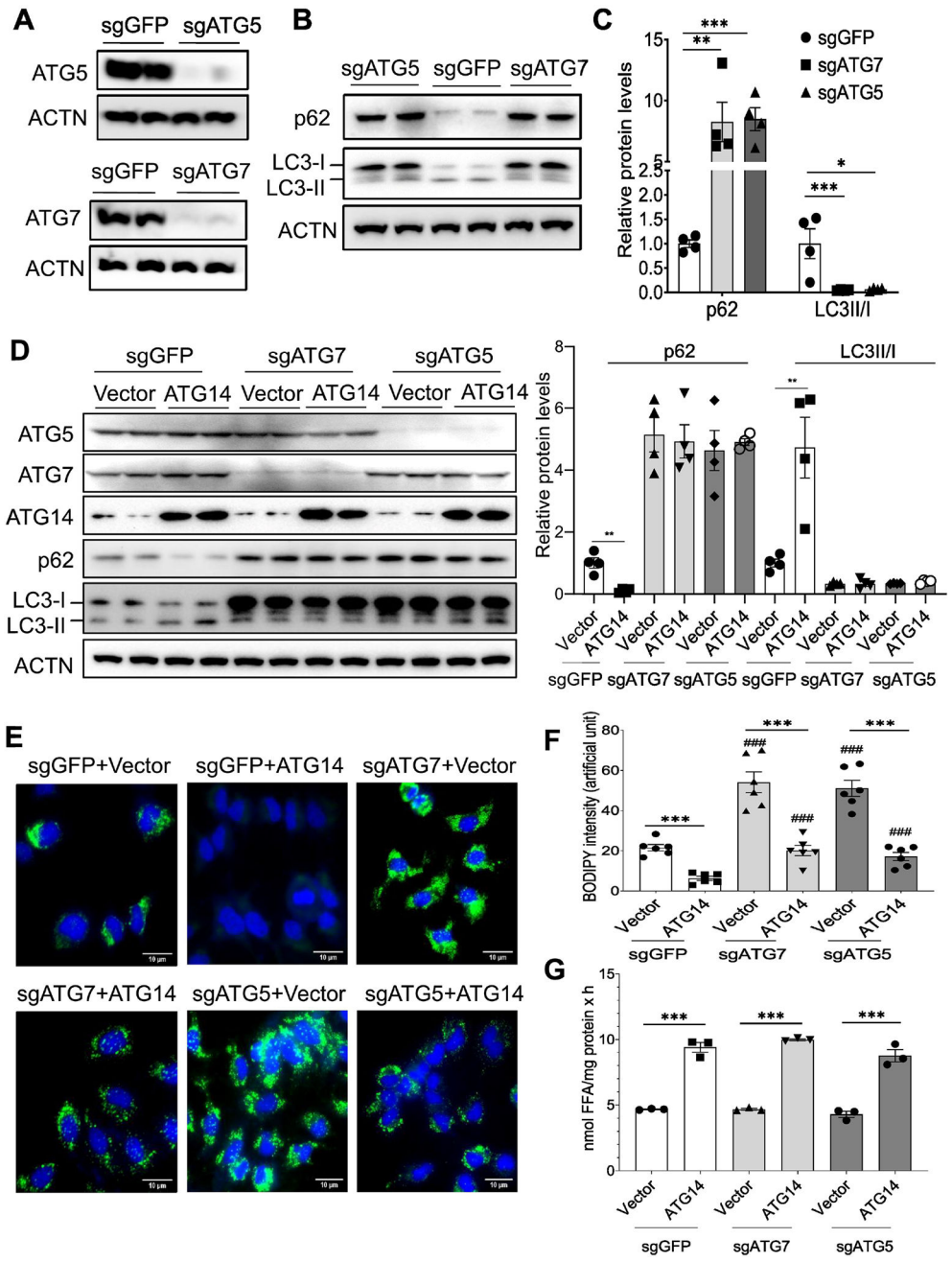


**Figure 10. ATG14 promotes triglyceride hydrolase activity in an autophagy-independent manner.**

(A-C) Immunoblot and quantification analysis of autophagy proteins in Huh-7 cells deficient in ATG5 or ATG7. (D) Immunoblot analysis ATG5, ATG7, ATG14, p62, and LC3-I/II proteins in Huh-7 cells transfected with the indicated plasmids (n = 4). (E-G) BODIPY staining and TG hydrolase activity analysis in Huh-7 cells with simultaneous ATG14 overexpression and ATG5 or ATG7 knockdown. Data are presented as mean ± SEM. *P < 0.05, **P < 0.01, and ***P < 0.001; ###P<0.001 vs. sgGFP.